Shielding Active Shape Models against Weak Lung Field Boundaries for Segmentation of Chest Radiographs

Michalis A. Savelonas, Dimitris K. Iakovidis

Dept. of Informatics and Comp. Technology, Technol. Educ. Institute of Lamia, Greece

Abstract. A novel active shape model (ASM) segmentation scheme is proposed, for the detection of the lung field boundaries in chest radiographs. The proposed scheme is robust in the presence of weak lung field boundaries, which are recognized as a common cause of missegmentation. This situation is prevalent in chest radiographs obtained from patients with abnormalities, such as lung consolidations, or even in normal chest radiographs of low quality. In order to shield the ASM against the presence of weak boundaries, the distance used in searching for the optimal displacements of the ASM landmarks is modified so that it incorporates both shape prior and patient-specific anatomical information. The segmentation performance of the proposed scheme is experimentally validated on a challenging set of chest radiographs obtained from patients with bacterial pulmonary infections. The results obtained indicate its advantage over the original ASM.

1 Introduction

A significant research effort has been invested in the segmentation of chest radiographs [1], including rule-based methodologies [2], neural network, Markov random fields [3] and other pattern classification approaches [4], active contour models [5], active shape models [6],[7] and graph cuts [8]. However, accurate segmentation of lung field boundaries defined by weak edges remains an open issue. Such weak edges are associated with the presence of abnormalities or with poor imaging quality and can be hardly distinguished even by experienced physicians [9].

Recently, a rule-based selective thresholding approach coping with the issue of weak edges has been proposed in [10]. This approach is unsupervised and defines a set of salient control points around the lung fields. The salient point detection process is supported by a selective thresholding algorithm that cuts off image intensities based on local intensity histograms sampled from the spinal cord. The detected points are then intuitively interpolated by Bézier curves [11]. The preliminary results presented indicate its robustness against the presence of weak edges, as well as its advantage against the graph cuts approach [8]. A drawback of this methodology is that it may produce implausible shapes, as a result of the shape variability characterizing lung field boundaries in chest radiographs.

Among the various lung field segmentation methodologies, the shape-constrained deformability of ASMs makes them a competent candidate for coping with the shape variability of the lung fields. According to the original ASM approach [12] the shape

of an image region is represented by the principal components of landmark point vectors, whereas the grey-level appearance of that region is limited to its border. The latter consists of the normalized first derivative of the grey-level intensity profiles centered at each landmark that run perpendicular to the region's contour. This formulation makes it evident that ASMs are quite sensitive to weak lung field boundaries, which affect the derivatives of the intensity profiles.

In this paper, a novel ASM-based segmentation scheme is proposed for the detection of lung field boundaries in chest radiographs, which copes with the presence of weak edges. The proposed scheme introduces a modified distance measure guiding the evolution of the ASM, which utilizes patient-specific anatomical information derived from the rule-based selective thresholding approach [10], so as to provide robustness against the presence of weak lung field boundaries. The ASM formulation of the proposed scheme accounts for the shape variability of the lung fields. The segmentation performance of the proposed scheme is experimentally validated on a challenging set of chest radiographs obtained from patients with bacterial pulmonary infections.

The rest of this paper consists of four sections. In section 2 a brief description of the utilized rule-based selective thresholding approach is provided. The modified ASM approach is presented in Section 3. In Section 4 the results of its experimental evaluation are presented, whereas in the last section the conclusions of this study are summarized.

2 Rule-Based Selective Thresholding

Let I be a new chest radiograph of size $N \times M$ pixels, which is uniformly sampled from top to bottom with s_h non-overlapping rectangular windows of $h \times M$, pixels, where $h<N$. For each sample an average horizontal profile of grey-level intensities is estimated. For each profile a local maximum is selected as a spinal cord point according to [10]. The selective thresholding algorithm proceeds as follows:

Step 1. Sample the radiograph across spinal cord:
- For each of the s_h points detected on the spinal cord:
  - Acquire a square sample of x^2 pixels.
  - For each sample $i=1,\ldots, s_h$:
    - Calculate its intensity histogram h_i,
    - Select a set of histogram components ph_i centered at its highest peak.

Step 2. Accumulate the values ph_i from all samples into a single histogram H.

Step 3. Find the last non-zero component m of H.

Step 4. Generate an output image $T(I)$ from I as follows:
- Set the intensities of I that correspond to the non-zero components of H, to zero.
- Set the intensities of I that are larger than m, to zero.
- Set all non-zero intensities to one to obtain a binary image.

The intensities that are larger than m are subtracted from I because they are unlikely

to belong to the lung fields since the spinal cord is generally brighter than both normal lung parenchyma and consolidations [13]. Such regions may include dense objects used for patient's monitoring or support. Figure 1 illustrates an example of a chest radiograph as well as the resulting thresholded image.

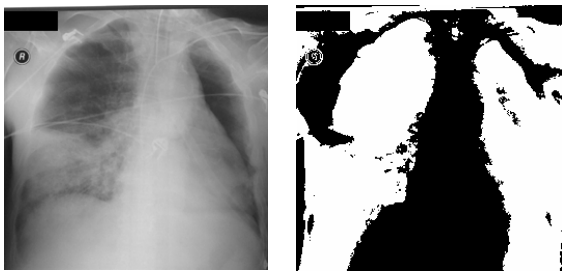

(a) (b)

Fig. 1. Example image. (a) Radiograph *I*, (b) Thresholded image *T*(*I*).

3 ASM Evolution guided by a Modified Distance Measure

The ASM approach [12] captures shape variability of the lung fields by applying principal component analysis (PCA) to build a shape model from a set of training shape vectors, which encode ground truth lung field boundaries. Shape vectors are defined as $\mathbf{x}=(x_1,y_1,\ldots,x_n,y_n)^{\mathrm{T}}$, where $(x_1,y_1),\ldots,(x_n,y_n)$ are n landmark points. The shape model is represented by the covariance matrix of the shape vectors $\mathbf{C}_{\mathbf{x}}$ from which t eigenvectors ϕ_i, i=1,…,t corresponding to the largest eigenvalues λ_i, are estimated.

The value of t is determined as the smallest t for which the following inequality holds [14]:

$$\sum_{i=1}^{t} \lambda_i \geq f_v \sum_{i=1}^{2n} \lambda_i \qquad (1)$$

where f_v is the desired percentage of shape variation to be represented by the t principal eigenvectors. The eigenvectors form the matrix $\Phi = (\phi_1|\phi_2|..|\phi_t)$ which is used for the approximation of a shape $\mathbf{x}$ in

$$\mathbf{x} = \bar{\mathbf{x}} + \Phi \cdot \mathbf{b}_{\mathbf{x}} \qquad (2)$$

where $\bar{\mathbf{x}}$ denotes the mean of N training shape vectors, and $\mathbf{b}_{\mathbf{x}}$ holds the shape parameters, estimated by $\mathbf{b}_{\mathbf{x}} = \Phi^{\mathrm{T}}(\mathbf{x} - \bar{\mathbf{x}})$.

In addition to the shape, the ASM models the local appearance of the image region around each landmark. The local appearance model is represented by the mean $\bar{\mathbf{d}}_i$ and the covariance matrix $\mathbf{C}_{\mathbf{d}i}$ of the normalized first derivatives $\mathbf{d}_i = (d_{i1}, d_{i2},..., d_{i2k})^{\mathrm{T}}$, k>0, of image intensity profiles $\mathbf{g}_i = (g_{i1}, g_{i2},..., g_{i2k+1})^{\mathrm{T}}$. The

latter are sampled around each landmark i=1,…,n over the N training shapes. The trained ASM is then applied on a new chest radiograph and evolves to detect the lung field boundaries.

The ASM evolves according to a simple iterative scheme [11]. Each landmark can move along a direction perpendicular to the contour by s positions on either side of the contour, evaluating 2s+1 positions, in total. In the original ASM formulation, the new position $(x'_{i,}y'_i)$ of each landmark i=1,…,n, on the search direction, is determined as the one minimizing the Mahalanobis distance $\mu(\mathbf{d}'_{ij})$ between the vector of the normalized first derivatives estimated from the 2s+1 pixel intensity profile centered at each of the possible new landmark positions $(x'_{ij,}y'_{ij})$, i=1,…,n, j=1,…,2s+1, and $\overline{\mathbf{d}}_i$:

$$\mu(\mathbf{d}'_{ij}) = (\mathbf{d}'_{ij} - \overline{\mathbf{d}}_i)^{\mathrm{T}} \mathbf{C}_{\mathbf{d}i}^{-1} (\mathbf{d}'_{ij} - \overline{\mathbf{d}}_i) \quad (3)$$

After all the landmarks are updated, the shape model is fitted to the new landmarks. It is evident that the Mahalanobis distance is sensitive to weak lung field boundaries, since the derivatives of the intensity profiles are affected.

The proposed ASM scheme utilizes a modified distance measure μ_a, which incorporates intensity gradient prior information quantified by Mahalanobis distance μ, as well as patient-specific anatomical information derived from the thresholded image $T(I)$ generated by the rule-based selective thresholding approach described in Section 2. The modified distance μ_a is defined as follows:

$$\mu_a = \mu + \lambda d \quad (4)$$

where λ is a weight parameter and d is the Euclidean distance between each of the possible new landmark positions $(x'_{ij,}y'_{ij})$ and the transition point (x_i^{tr}, y_i^{tr}), i=1,…,n, j=1,…,2s+1. The latter is defined for each landmark i, as the closest point to i along the direction perpendicular to the contour, which is associated with an intensity transition on the thresholded image $T(I)$.

Intuitively, Eq. (4) is based on the consideration that in cases of weak lung field boundaries μ is expected to be less discriminative due to its dependence on the normalized first derivatives. However, among the new candidate landmark positions, the one associated with the smaller Euclidean distance d, is more likely to correspond to the actual lung field boundaries. Thus, the patient-specific anatomical information provided by $T(I)$, complements the intensity gradient prior information quantified by μ and allows μ_a to provide a more complete measure of the likelihood of a candidate landmark position to correspond to the actual lung field boundaries.

The incorporation of a multiresolution local appearance model helps the algorithm to avoid trapping into irrelevant regions, whereas the intensity gradient prior information included in the ASM contributes to the plausibility of the output lung field shapes.

The algorithm of the proposed ASM scheme proceeds as follows:

Step 1. Update landmark positions:

- For each possible new landmark position $(x'_{ij,}y'_{ij})$, i=1,…,n, j=1,…,2s+1:
  - Calculate a profile of normalized first derivatives

$\mathbf{d}'_{ij} = (d_{ij1}, d_{ij2}, ..., d_{ij2k})^{\mathrm{T}}$ on I, centered at this landmark position perpendicular to the contour.

- Calculate the modified distance $\mu_a(\mathrm{d}'_{ij})$.
- Find $\mu_{\min}(\mathrm{d}'_i) = \min_{j=1,...,2s+1}(\mu_a(\mathrm{d}'_{ij}))$.
- Set $(x'_i, y'_i) = (x'_{ij}, y'_{ij})$ as the new position of landmark i.

Step 2. Fit the current shape model to the updated landmarks:

- Set $\mathbf{x}' = (x'_1, y'_1, ..., x'_n, y'_n)^{\mathrm{T}}$.
- Calculate the new model parameters for $\mathbf{x}'$ by solving Eq. (2) for $\mathbf{b}_{\mathbf{x}'}$.
- Constrain each component $|b_l| < c\sqrt{\lambda_l}$ of $\mathbf{b}_{\mathbf{x}'}$, c>0, l=1,…t, to ensure plausible shapes.

Step 3. Repeat steps 1 to 3 until a proportion p_{close} of points ends up within s/2 of its previous position, or $M_{\max}$ iterations are reached.

Step 4. Move to the next resolution level.

Step 5. Repeat steps 1 to 4 until the finest resolution level $R_{\max}$ is reached.

4 Results

The experimental evaluation of the proposed approach was performed on a set of 96 anonymous chest radiographs obtained with a portable x-ray device from 24 critically ill patients with pulmonary bacterial infections manifested as consolidations. For each patient, a sequence of four chest radiographs was obtained, depicting the progress of the infection at different stages.

Each sequence used in the experiments was obtained after the results of microbiological culture had been issued and the appropriate treatment had been prescribed. As a result of the treatment, in all 24 used sequences the infection diminished with time, the consolidations gradually disappeared and the edge strength associated with lung field boundaries increased. Figure 2 illustrates an example of such a sequence.

All radiographs used in the experiments where digitized at 8 bits and have been downscaled to fit a 256×256-pixel bounding box. Initial pilot experiments which were performed on the complete dataset of 96 images revealed that the image downsampling does not significantly affect the obtained segmentation performance, whereas it reduces the execution time of the algorithm. In addition, these pilot experiments allowed the selection of a fixed shape model parameter setting that yielded good performance. A shape model explaining 98% of the variance (f_v=0.98) was constructed based on the application of PCA on the set of 96 training shape vectors associated with ground truth lung field boundaries, as described in Section 3.

Other settings include three levels of resolution (R_{max}=3), thirty iterations per resolution level (M_{max}=30) and search regions associated with profiles of length five (s=2). When fitting the shape model to the displaced landmarks, each mode was constrained within two times (c=2) the standard deviation. The weight parameter was set equal to one (λ=1), considering the results derived for λ=0.5, 1, 1.5, which indicate

that the influence of the two terms in (4) is approximately equal. Additional values of parameters associated with the sizes used for the salient point detection and selective thresholding include h=9 and x=32.

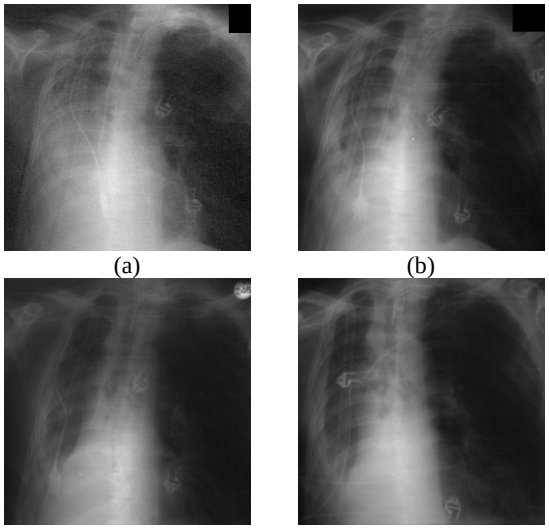

Fig. 2. Example sequence of 4 chest radiographs of the same patient, as the infection of the left lung is diminishing with time.

The performance of the proposed methodology was assessed in terms of Ω, a widely accepted measure of accuracy for binary segmentation tasks:

$$\Omega = \frac{TP}{TP + FP + FN} \quad (5)$$

where *TP* stands for true positive (the area classified as lung by both the proposed methodology and the expert), *FP* for false positive (area classified as background by the expert and as lung by the proposed methodology) and *FN* for false negative (area classified as lung by the expert and as background by the proposed methodology). This measure is a more suitable measure of segmentation performance than the accuracy used in [10], since the latter counts *TN* pixels as correctly detected, providing deceptively high results in cases of relatively small target objects.

A cross-validation scheme involving a total of 24 experiments was employed for the evaluation of the proposed scheme and the original ASM. In each experiment, 92 images comprising of 23 sequences of 4 images each, were used for training, whereas the remaining 4 images of the dataset, which did not belong to the training set and were associated with the same sequence, were used for testing.

Figure 3 presents the progress in time of the mean Ω, obtained as the infection was diminishing, by using the proposed scheme and the original ASM. The value i of the horizontal axis corresponds to the i-th images of all 24 time-sorted sequences, i=1,…,4. Considering that the infections were diminishing with time for all sequences

used, as i increases the mean Ω is calculated over images of increasing density of consolidations. The results indicate that: a) the proposed scheme achieves higher Ω than the original ASM, b) mean Ω obtained by the proposed scheme exceeds 0.85 for all levels of consolidation densities, c) the difference of mean Ω obtained by the proposed scheme and the original ASM is higher in the first images of the sequences, were the density of consolidations is higher.

Figure 4 illustrates the segmentation results obtained by the application of the proposed scheme and the original ASM on the sequence of Fig. 2. It can be observed that unlike the original ASM, the proposed segmentation scheme avoids contour leaking, even in cases of lung field boundaries characterized by weak edges (Fig, 4a1).

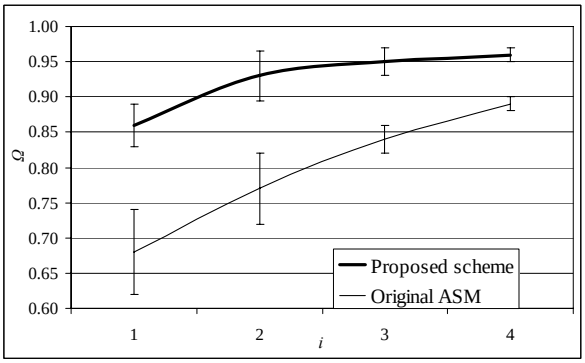

Fig. 3. Progress in time of the mean Ω, obtained as the infection was diminishing.

5 Conclusion

We presented a novel ASM-based segmentation scheme for robust detection of the lung field boundaries in chest radiographs. The proposed scheme utilizes a modified distance measure that incorporates both intensity gradient prior and patient-specific anatomical information to obtain insensitivity to the presence of weak boundaries. The results of its experimental evaluation lead to the following conclusions:

- It achieves more accurate detection of the lung field boundaries than the original ASM.
- It provides robust segmentation of the lung fields in the presence of weak boundaries.
- Its advantageous segmentation performance becomes more evident as the lung field boundaries become weaker.

The proposed scheme introduces a framework, which could potentially embed alternative feature vectors, such as the feature vector calculated by the application of the modified scale invariant feature transform (SIFT). SIFT is supported by recent studies [15] as more distinctive than the general intensity and gradient features. Future work also includes a thorough investigation of the impact of various parameter values on the results and the integration of the proposed lung field detection scheme into a multimodal data mining system for adverse events detection, which will be

capable of co-evaluating radiographic findings of patients with bacterial infections [16].

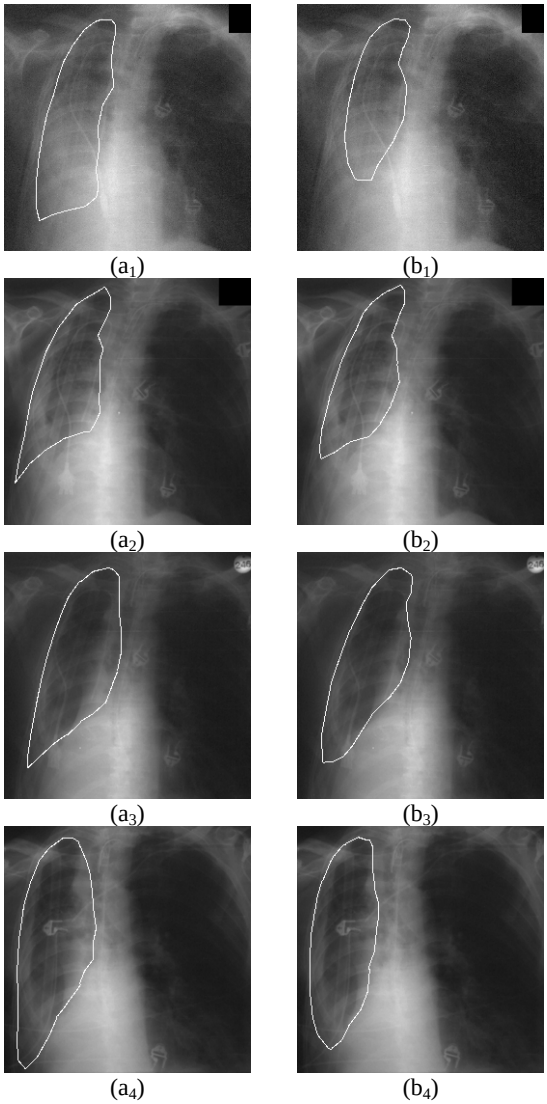

Fig. 4. Segmentation results obtained by the application of the proposed scheme (a_1-a_4) and the original ASM (b_1-b_4) on the sequence of Fig. 2.

Acknowledgement

Great thanks to Dr. G. Papamichalis, M.D. who generously offered his help and advice on the medical aspects of this study. The radiographs have been provided in

anonymized form by the General Hospital of Athens “Sotiria” for the purposes of the project DEBUGIT. This work was supported in part by the European Commission’s Seventh Framework Information Society Technologies (IST) Programme, Unit ICT for Health, project DEBUGIT (no. 217139).

References

1. Ginneken B.V., Romeny B.T.H., Viergever M.A.: Computer-Aided Diagnosis in Chest Radiography: A Survey. IEEE Trans. Medical Imaging, Vol. 20, No. 12 (2001) 1228-1241
2. Ginneken B.V., Romeny B.T.H.: Automatic Segmentation of Lung Fields in Chest Radiographs. Medical Physics, Vol. 27, No. 10 (2000) 2445-2455
3. McNitt-Gray M.F., Huang H.J., Sayre J.W.: Feature Selection in the Pattern Classification Problem of Digital Chest Radiograph Segmentation. IEEE Trans. Medical Imaging, Vol. 14, No. 3 (1995) 537–547
4. Vittitoe N., Vargas-Voracek R., Floyd C. Jr: Markov Random Field Modeling in Posteroanterior Chest Radiograph Segmentation. Medical Physics, Vol. 26, No. 8 (1999) 1670-1677
5. Coppini G., Diciotti S., Falchini M., Villari N., Valli G.: Neural Networks for Computer-Aided Diagnosis: Detection of Lung Nodules in Chest Radiograms. IEEE Trans. Information Technology in Biomedicine, Vol. 7, No. 4 (2003) 344-357
6. Ginneken B.V., Stegmann M.B., Loog M.: Segmentation of Anatomical Structures in Chest Radiographs using Supervised Methods: A Comparative Study on a Public Database. Medical Image Analysis, Vol. 10 (2006) 19-40
7. Ginneken B.V., Frangi A.F., Staal J.J., Romeny B.T.H., Viergever M.A.: Active Shape Model Segmentation with Optimal Features. IEEE Trans. Medical Imaging, Vol. 21 (2002) 924-933
8. Chen S., Cao L., Liu J., Tang X.: Automatic Segmentation of Lung Fields from Radiographic Images of SARS Patients Using a New Graph Cuts Algorithm. Proc. Int. Conf. Pattern Recognition (ICPR), Vol. 1 (2006) 271-274
9. Müller N.L., Franquet T., Lee K.S., Isabela C.: Silva S.: Imaging of Pulmonary Infections, Lip. Williams & Wilkins (2006)
10. Iakovidis D.K., Papamichalis G.: Automatic Segmentation of the Lung Fields in Portable Chest Radiographs Based on Bézier Interpolation of Salient Control Points. Proc. IEEE Int. Conf. Imag. Sys. Tech., Greece (2008) 82-87
11. Bartels R.H., Beatty J.C., Barsky B.A.: An Introduction to Splines for Use in Computer Graphics and Geometric Modelling. San Francisco, CA: Morgan Kaufmann (1998) 211-245
12. Cootes T., Taylor C., Cooper D., Graham J.: Active Shape Models - Their Training and Application. Computer Vision and Image Understanding, Vol. 61, No. 1 (1995) 38-59
13. Novelline R.A.: Squires’s Fundamentals of Radiology. Cambridge: Harvard University Press (1997)
14. Ginneken B.V., Katsuragawa S., Romeny B.T.H., Doi K., Viergever M.A.: Automatic Detection of Abnormalities in Chest Radiographs Using Local Texture Analysis. IEEE Trans. Medical Imaging, Vol. 21, No. 2 (2002) 139-149
15. Shi Y., Qi F., Xue Z., Chen L., Ito K., Matsuo H., Shen D.: Segmenting Lung Fields in Serial Chest Radiographs Using Both Population-Based and Patient-Specific Shape Statistics. IEEE Trans. Medical Imaging, Vol. 27, No. 4 (2008) 481-494
16. Lovis C., Colaert D., Stroetmann V.N.: DebugIT for Patient Safety-Improving the Treatment with Antibiotics through Multimedia Data Mining of Heterogeneous Clinical Data, Stud. Health Technol. Inform., Vol. 136 (2008) 641-646